



**Scattering Particles Increase Absorbance of Dyes – A Model  
Study with Relevance for Sunscreens**

Journal:	<i>Photochemical &amp; Photobiological Sciences</i>
Manuscript ID:	PP-ART-03-2015-000109.R2
Article Type:	Paper
Date Submitted by the Author:	18-Aug-2015
Complete List of Authors:	Herzog, Bernd; BASF Grenzach GmbH, Sengün, Fazilet; University of Basel, Pharmaceutical Technology



Journal Name

ARTICLE

## Scattering Particles Increase Absorbance of Dyes – A Model Study with Relevance for Sunscreens

Bernd Herzog<sup>a</sup> and Fazilet Sengün<sup>b</sup>

Received 00th January 20xx,  
Accepted 00th January 20xx

DOI: 10.1039/x0xx00000x

www.rsc.org/

Sunscreens used for the protection of human skin against the harmful effects of solar radiation contain UV absorbers as key ingredients, which are either dissolved in one of the phases of the preparation or, when insoluble, suspended as particles. Although the UV protective effect of particulate UV filters, inorganic and organic, is mainly due to absorption, they scatter UV and visible light. The scattering can have an additional attenuating effect on the incoming radiation by increasing the pathlength of the photons, especially when soluble filters are also present. This is investigated with model systems of dyes and absorbing and non-absorbing particles. The presence of particles causes an increase of the dye absorbance without changing dye concentration or cuvette thickness. It is possible to relate this amplification of dye absorbance to the turbidity of the system. Plots are constructed which allow for a given particle type the representation of all data on one single curve, though measured at different turbidity and cuvette thickness. With that, extrapolations to practical applications of sunscreens are possible.

### Introduction

Sunscreens used for the protection of human skin against the harmful effects of solar radiation often contain significant amounts of UV absorbing substances. However, the concentrations of individual UV absorbers in sunscreen compositions are limited [1] due to weak solubility, regulatory reasons or patent restrictions, and it is desirable to explore possibilities how most efficient sunscreens may be composed. Besides organic oil- or water-soluble UV absorbers, also inorganic or organic particulate UV-absorbers are often employed as UV filtering materials [2], such as TiO<sub>2</sub> and ZnO, or methylene-bis-benzotriazolyl tetramethylbutylphenol (MBBT) and tris-biphenyl triazine (TBPT), respectively. The latter ones are of extremely poor solubility in water and cosmetic oils [2, 3], and are prepared in the form of aqueous dispersions. The two mentioned inorganic oxides may be dispersible in either water or oils via adapted coatings [4].

All particulate UV filters in sunscreens have in common that their protective effect is mainly due to absorption of UV photons. In comparison, attenuation of UV light by scattering only plays a minor role. For instance, the scattering coefficient

of MBBT particles is about one tenth of the absorption coefficient of that material [5]. Nevertheless, due to scattering, light is diffused in different directions when such particles are present. This effect leads to an increase of the effective optical pathlength of the incoming radiation and thus also to a higher probability for absorption to take place, especially when soluble UV absorbers are dissolved in the medium. For that reason, a certain amplification effect in terms of UV absorption should be observed when particles are present in a sunscreen. This effect can equally be expected with particles which do not absorb but only scatter the radiation, such as polymer spheres. In an analogous manner the principle of increasing the light absorption of dyes by addition of scattering particles is exploited in dye-sensitized solar cells [6].

The aim of the present work is to investigate how scattering of particles can increase the action of the UV-absorbing substances which are present in the same medium. As one of the particles is a UV absorber itself, the effect is investigated with water-soluble dyes instead of UV absorbers, as dyes show an absorption band in the visible range which will not interfere with the UV absorption one type of the particles shows.

### Theoretical considerations

In transmittance measurements of light absorbing molecules dissolved in a suitable liquid medium, the absorbance  $A(\lambda)$  depends linearly on the optical thickness  $d$ , which is given as the inner distance between front and back window of a cuvette placed in the light beam of the spectrometer, as expressed in the Beer-Lambert-law:

<sup>a</sup> BASF Grenzach GmbH, G-9001.2.28, Köchlinstrasse 1, 79639 Grenzach-Wyhlen, Germany, e-mail: bernd.herzog@basf.com

<sup>b</sup> University of Basel, Institute of Pharmaceutical Technology, Klingelbergstrasse 50, 4056 Basel, Switzerland, e-mail: fa.senguen@gmail.com

† Footnotes relating to the title and/or authors should appear here. Electronic Supplementary Information (ESI) available: [details of any supplementary information available should be included here]. See DOI: 10.1039/x0xx00000x

$$A(\lambda) = \varepsilon(\lambda) \cdot c \cdot d \quad (1)$$

where  $\varepsilon(\lambda)$  is the absorption coefficient,  $\lambda$  the wavelength of the radiation and  $c$  the molar concentration of the absorbing substance. The transmittance  $T(\lambda)$  is the ratio of transmitted and incoming light intensities,  $I_t(\lambda)$  and  $I_0(\lambda)$ , respectively, and the relationship of transmittance and absorbance is given in equation (2):

$$A(\lambda) = -\log_{10}(T(\lambda)) \quad (2)$$

If particles (here typically in a size range between 10 and 500 nm) are present in the same medium, they may scatter the light. This gives rise to an attenuation of the light beam when passing through the sample, designated as turbidity  $\tau(\lambda)$ :

$$\tau(\lambda) = d^{-1} \ln(I_0(\lambda)/I_t(\lambda)) \quad (3)$$

Most of the light scattered by the particles will have other directions than the incoming beam, and part of it being scattered in forward direction, part in backward direction (Figure 1). Any deviation in forward direction with respect to the incident direction will result in a longer path of the light when passing through the sample. This will be even more the case when multiple scattering events will take place (like in the systems considered here).

When dye molecules are dissolved in the medium, the presence of suspended particles will thus increase the effective pathlength of the light and the probability of absorption by the dyes, resulting in an augmented dye absorbance. This effect will depend on the turbidity of the sample due to the presence of particles in the medium. When the particle concentration is high enough to allow multiple light scattering, the movement of the photons can be viewed as a diffusion process [7]. Considering diffusion of matter, this can be described as random walk with the result, that the average displacement of the diffusing object is proportional to the square root of the product of diffusion coefficient and time [8]. In analogy, regarding a random walk of photons through a turbid medium in a cuvette of thickness  $d$ , having entered the cuvette as a directed beam of light, it is assumed that the distance the photons have to pass until leaving the cuvette at the opposite site will be proportional to the square root of the product of turbidity of the medium and cuvette thickness. On the other hand, when light absorbing molecules, such as dyes, are present as well, the diffusion process will be dampened as light will be absorbed. Thus it is expected that the amplifying effect due to the presence of scattering particles will be a function of  $(\tau \cdot d / A_0(\lambda))^{1/2}$ , where  $A_0(\lambda)$  is the absorbance due to the dye absorption when no particles are present, and our hypothesis is expressed by the equation (4):

$$A_p(\lambda) / A_0(\lambda) = f(\sqrt{(\tau(\lambda) \cdot d) / A_0(\lambda)}) \quad (4)$$

where  $A_p(\lambda)$  is the absorbance in the presence of particles. The form of equation (4) leaves it open whether the relationship is linear or of a different functionality. The turbidity of the particle suspension can be obtained via the Rayleigh ratio for unpolarised light  $R(q)$  according to equation (5) [9]:

$$\tau(\lambda) = 2\pi \int_0^\pi R(q) \sin\theta d\theta \quad (5)$$

where  $\theta$  is the scattering angle and  $q$  the scattering vector:

$$q = \frac{4\pi n_0}{\lambda} \cdot \sin(\theta/2) \quad (6)$$

with the refractive index of the medium  $n_0$ . The Rayleigh-ratio is calculated according to the Rayleigh-Gans-Debye approximation [9, 10]:

$$R(q) = Kc \cdot (n_0\pi D/\lambda)^3 \cdot P(q) \cdot S(q) \cdot (1 + \cos^2\theta) \quad (7)$$

where  $K$  is the optical constant,  $c$  the concentration of the particles,  $D$  their diameter,  $P(q)$  the form factor and  $S(q)$  the structure factor. The optical constant is given as

$$K = \frac{3n_0}{4\lambda\rho_p} \left( \frac{m^2-1}{m^2+2} \right) \quad (8)$$

where  $\rho_p$  is the density of the particles and  $m = n_p/n_0$ , with  $n_p$  the refractive index of the particles. The dispersion of the refractive index was fitted to experimental data at six wavelengths using equation (9) [11]:

$$m(\lambda) = \sqrt{1 + \frac{a\lambda^2}{\lambda^2 - b}} \quad (9)$$

with  $a$  and  $b$  as adjustable parameters.

Using the volume fraction  $\varphi = c/\rho_p$ , equation (5) gets the form:

$$\tau(\lambda) = 12\varphi \cdot \left( \frac{m^2-1}{m^2+2} \right) \left( \frac{n_0\pi}{\lambda} \right)^4 \cdot R^3 \cdot \int_0^\pi P(q) \cdot S(q) \cdot (1 + \cos^2\theta) \cdot \sin\theta d\theta \quad (10)$$

where  $R$  is the particle radius.

The particle form factor  $P(q)$  for spheres [12] is calculated according to the following expression:

$$P(q) = \left\{ \frac{3}{(q \cdot R)^3} \cdot [\sin(q \cdot R) - q \cdot R \cdot \cos(q \cdot R)] \right\}^2 \quad (11)$$

In equations (7) and (10) the structure factor  $S(q)$  is also considered [13], which gets important at higher volume fractions:

$$S(q) = \frac{1}{1-F(q)} \quad (12),$$

and

$$F(q) = \frac{-24 \cdot \varphi \cdot \left\{ L_1 \cdot \left[ \frac{\sin(q \cdot D) - q \cdot D \cdot \cos(q \cdot D)}{(q \cdot D)^3} \right] - 6 \cdot \varphi \cdot L_2 \cdot \left[ \frac{(q \cdot D)^2 \cdot \cos(q \cdot D) - 2 \cdot q \cdot D \cdot \sin(q \cdot D) + 2 \cdot \cos(q \cdot D) + 2}{(q \cdot D)^4} \right] - \varphi \cdot \frac{L_1}{2} \cdot \left[ \frac{(q \cdot D)^4 \cdot \cos(q \cdot D) - 4 \cdot (q \cdot D)^3 \cdot \sin(q \cdot D) - 12 \cdot (q \cdot D)^2 \cdot \cos(q \cdot D) + 24 \cdot q \cdot D \cdot \sin(q \cdot D) + 24 \cdot \cos(q \cdot D) - 24}{(q \cdot D)^6} \right] \right\}}{(12a),$$

Where  $D = 2 \cdot R$ , and

$$L_1 = \frac{(1+2 \cdot \varphi)^2}{(1-\varphi)^4} \quad \text{and} \quad L_2 = \frac{-(1+\varphi/2)^2}{(1-\varphi)^4} \quad (12b).$$

The integral expression in equation (10) is evaluated numerically using Microsoft EXCEL 2010.

In the following, turbidities are calculated according to equation (10). They are later used to check the relationship expressed in equation (4). In order to verify the calculated turbidities, they are compared with turbidity measurements on pure particulate systems without dye. The schematic experimental set-up for such measurements is shown in Figure 2a. No integrating sphere is used in this case. The corresponding results are depicted in Figures 5 and 6.

For the investigation of the increase of dye absorbance expected in samples containing dye and particles, the set-up schematically drawn in Figure 2b is employed. Here an integrating sphere is used in order to detect the light scattered in forward direction, such that dye absorbance will be the main cause for the reduction of transmitted intensity. As there is also back-scattering, which is not detected by the integrating sphere, a reference containing only the corresponding particle suspension was measured in parallel under the same conditions and subtracted from the sample measurement.

## Materials and methods

### Chemicals

#### Particles

Spherical polymer particles consisting of a styrene-acrylate copolymer were used as model scatterers (Sunspheres PGL™, Dow Chemicals). The product is described [14] as hollow spheres with an outer diameter of 350 nm and a thick shell. The particles were obtained as a 25.5% (w/v) aqueous dispersion at neutral pH, which was further diluted to the concentrations needed in our experiments. The density of the polymer spheres is given as  $1.10 \text{ g/cm}^3$ .

An organic particulate UV absorber (Tinosorb M™, BASF) was used as further scattering system. The product consists of an aqueous dispersion of 50% methylene-bis-benzotriazolyl tetramethylbutylphenol (MBBT) particles with a broad size distribution and a median particle size of about 160 nm [15]. The dispersion also contains 7.5% decyl glucoside, 0.2% xanthan

gum and 0.4% propylene glycol. The product will be referred to in the following as MBBT particles. The density of the particles had been determined by sedimentation studies with solid MBBT in glucose solutions of different densities to  $1.12 \text{ g/cm}^3$  [16].

### Water-soluble dyes

Five water-soluble dyes were used ( $\varepsilon$  = molar decadic absorption coefficient,  $\lambda_{\text{max}}$  = wavelength of maximum absorption at pH = 7):

Eosin Yellow (alternative name Acid Red 87); the chemical name is disodium 2-(2,4,5,7-tetrabromo-6-oxido-3-oxoxanthene-9-yl)benzoate, from Sigma-Aldrich;  $\varepsilon = 85500 \text{ L mol}^{-1} \text{ cm}^{-1}$ ,  $\lambda_{\text{max}} = 517 \text{ nm}$ .

Evans Blue (alternative name Direct Blue 53); the chemical name is tetrasodium 6,6'-((3,3'-dimethyl-(1,1'-biphenyl-4,4'-diyl)bis(azo)bis(4-amino-5-hydroxy-1,3-naphthalenedisulphonate), from ABCR GmbH & Co. KG;  $\varepsilon = 75700 \text{ L mol}^{-1} \text{ cm}^{-1}$ ,  $\lambda_{\text{max}} = 604 \text{ nm}$ .

Malachite Green (alternative name Basic Green 4); the chemical name is 4-[[4-(dimethylamino)phenyl](phenyl)methylidene]-N,N-dimethylcyclohexa-2,5-dien-1-iminium chloride, from Riedel de Haen;  $\varepsilon = 151700 \text{ L mol}^{-1} \text{ cm}^{-1}$ ,  $\lambda_{\text{max}} = 617 \text{ nm}$ .

Patent Blue V (alternative name Acid Blue 3); the chemical name is 2-[[4-(diethylaminophenyl)(4-diethylimino-2,5-cyclohexadien-1-ylidene)methyl]-4-hydroxy-1,5-benzene-disulfonate, from Sigma Aldrich;  $\varepsilon = 113900 \text{ L mol}^{-1} \text{ cm}^{-1}$ ,  $\lambda_{\text{max}} = 637 \text{ nm}$ .

Direct Red 254 (alternative name Pergasol Red 2B); the chemical name is 7-amino-4-hydroxy-3-((4-((4-sulphophenyl)azo)phenyl)azo)naphthalene-2-sulphonic acid; from BASF;  $\varepsilon = 22200 \text{ L mol}^{-1} \text{ cm}^{-1}$ ,  $\lambda_{\text{max}} = 504 \text{ nm}$ .

UV/vis absorbance spectra of those dyes were measured in aqueous solutions buffered with phosphate buffer at pH 7 and are shown in Figure 3. The absorption coefficients given here are based on these measurements.

### Other chemicals

De-ionized water was used in all experiments. Phosphate buffer solution at pH 7.0 and analytical grade was purchased from Fluka.

### UV/vis spectroscopic measurements

UV/vis-spectra of pure dye solutions were measured with a Perkin Elmer Lambda 650 UV/vis double-beam spectrometer without integrating sphere. The sample solution and the reference (pure solvent) were filled into quartz cells of 1 cm

optical pathlength and placed into the respective beams of the device. Turbidity spectra of mere particle dispersions were also measured with this spectrometer in quartz cuvettes of 0.1 cm optical path length (polymer spheres) or sandwich cuvettes of 0.0008 cm (MBBT particles) against corresponding reference cuvettes containing pure medium.

For measurements of dye solutions containing particles, a Perkin Elmer Lambda 20 UV/vis spectrometer with an integration sphere accessory (RSA-PE-20) was employed, in order to collect the direct transmitted light and also the light scattered in forward direction. Although the Perkin Elmer Lambda 20 is a double beam spectrometer, the integration sphere accessory is a single beam device. Thus, first a reference is measured and after that the corresponding samples. Reference and sample cells were placed in the light beam at the transmittance port of the integration sphere, while a reflectance standard was mounted at the reflectance port of the sphere. Measurements were performed with a spectral resolution of 2 nm. For absorbance measurements, dispersions were filled into quartz cuvettes (Hellma Analytics), which were available in a variety of thicknesses, such as 0.002 cm, 0.005 cm, 0.01 cm, 0.1 cm and 0.2 cm. The dispersions were produced in the following way: A stock solution of the respective dye was prepared. The concentrations of the dyes were adjusted such that absorbance values at the wavelength of maximum absorption were approximately 0.075, 0.15 or 0.3 in the absence of particles after addition of the other components, finally resulting in a twofold dilution of the stock solution. The corresponding dye concentrations were kept the same when particles were added. The dye solutions were prepared in 30 mM phosphate buffer at pH 7.0. Particle dispersions were prepared at various particle concentrations. In the case of the polymer spheres the 25.5% (w/v) aqueous dispersion was accordingly diluted with deionized water, in case of MBBT the 50% dispersion. Prior to measurements, 2.5 mL of the dye solution were added to 2.5 mL of the respective particle dispersion, resulting in a buffer concentration of 15 mM and also halving of the concentrations of the other components in the stock solutions. Reference samples for the UV/vis-spectroscopic measurements were prepared with the same particle concentrations, adding buffer solution without dye. Spectra were recorded in intervals of 1 nm in the range between 250 and 850 nm. As none of the used dyes absorbs at wavelengths greater than 750 nm, after subtraction of the reference measurement with the pure particle suspension the absorbance in the range above 750 nm should have been zero. This was not always exactly the case, and then a baseline correction was performed (by calculating the average absorbance in the range between 800 and 850 nm and subtracting this value from the absorbance values over the complete spectrum).

#### Light scattering measurements

##### Determination of particle scattering functions

Particle scattering functions were determined with goniometer-type light scattering measurements using an ALV-5000 instrument (ALV Laser Vertriebsgesellschaft). As light source served a 50 mW diode-pumped NdYAG laser (Uniphase), emitting light at a wavelength of 532 nm. The scattered light intensity was read and the value corrected for the angular dependence of the scattering volume by multiplying with  $\sin\theta$ . It was checked before, that this operation lead to a constant value when varying the scattering angle in a range between 20° and 150° with an aqueous solution of a fluorescing dye (Eosin Yellow) in the scattering cell. For the measurement of the particle scattering function of the polymer spheres, dispersions were diluted to 0.025 g/l using ionized water, and filtered through 0.8  $\mu\text{m}$  filters (MinisartR, Sartorius Sterile-EO) directly into dust-free scattering cells of 2.0 cm outer diameter (Hellma). The intensity of the scattered light was recorded at scattering angles between 15° and 155° at 5° steps. The temperature was held constant at 25°C.

##### Fibre-optic quasi-elastic light scattering (FOQELS)

FOQELS [17] is a dynamic light scattering technique operating at a scattering angle of 180°. This experimental setup enables measurements at high particle concentrations (> 1%) without multiple scattering problems since only back-scattered light of a thin particle layer is detected [18]. The light ( $\lambda = 632.8 \text{ nm}$ ) of a 15 mW He/Ne-laser (Spindler & Hoyer) is guided through a single mode optic fibre of 4  $\mu\text{m}$  diameter which is immersed in the particle dispersion. The ending of the fibre is ground to an angle 10° different from the normal to the optical axis in order to avoid heterodyne signals caused by back-reflected light from the quartz/water interface. Back-scattered light from the particles ( $\Theta = 180^\circ$ ) enters the fibre and is guided to the detector (ALV SO-SIPD Single Photon Detector, ALV Laser Vertriebsgesellschaft). The autocorrelator of the ALV 5000 device was used to build up the autocorrelation functions. Since only scattered light of a thin layer of particles is collected, concentrated suspensions may be measured without or only weak dilution. FOQELS measurements with the spherical polymer particles at concentrations between 1.3% and 2.7% (w/v) showed no concentration dependence. With MBBT this was the case at particle concentrations between 1% and 4% (w/v) [15]. Prior to the measurements diluted dispersions were treated with ultrasound for 60 seconds using an ultrasonic tip (Branson Model 250 Sonifier, output power 70 W) in order to break up aggregates. For each determination of the particle size distribution with FOQELS, four independent dilutions were prepared from the sample. With each particle dispersion three measurements were taken and the resulting distributions were averaged before calculating median-values (synonymous with d(0.5)-values) [15].

## Results and discussion

### Light scattering results with polymer spheres

The median value of the diameter determined with the FOQELS technique at a polymer particle concentration of 1.35% (w/v) resulted in a value of  $d(0.5) = 368 \text{ nm} \pm 12 \text{ nm}$  corresponding to a radius of 184 nm.

The particle form factor measured with the ALV 5000 device as described in the previous section was obtained by calculating the ratio of the scattering intensities  $I_\theta/I_0$ , where  $I_\theta$  is the scattering intensity at scattering angle  $\theta$ , corrected for the angular dependence of the scattering volume, and  $I_0$  is the scattering intensity at scattering angle 0. Equation (11) was fitted to the experimental data with a non-linear least-square fit (using the EXCEL solver) by adjusting  $I_0$  (which cannot be measured directly) and  $R$ , the radius of the spheres. The best fit was obtained with a sphere radius of 175 nm. This is in good agreement with the FOQELS result of 184 nm. Experimental data and the fit according to equation (11) are shown in Figure 4. It was also attempted to adjust the equation for the particle scattering function of hollow spheres with finite shell size [10] to the experimental data, but this did not lead to satisfactory agreement with the experimental data.

#### Turbidity of polymer sphere dispersions

The turbidity of the polymer spheres was measured at different particle concentrations in aqueous dispersion. With the particle density of  $\rho = 1.1 \text{ g/cm}^3$  the volume fraction  $\varphi$  was calculated as  $\varphi = \beta/(100 \rho)$ , where  $\beta$  is the particle concentration in percent (w/v). Refractive indices of polystyrene (PS) and polymethylmethacrylate (PMMA) were obtained from reference [11]. As the polymer spheres consist of a copolymer of PS and PMMA, the refractive index was calculated as the average of the values of the two materials at six wavelengths (Table 1). The spectral dispersion of the refractive index ratio  $m = n_p/n_0$  was approximated using equation (9), adjusting the parameters to values of  $a = 0.31447$  and  $b = 0.023776$ . The turbidity was calculated with equation (10) using a particle radius of 175 nm. In Figure 5 the result is shown for a volume fraction of  $\varphi = 0.001769$ . Since the measured and calculated data are based on different logarithms, see equations (2) and (3), the calculated data of  $\tau \cdot d$  have to be divided by  $\ln(10)$  in order to be comparable with experimental data. The agreement between measurements and calculation is good. The small deviations could be due to a different ratio of the PMMA and PS fractions in the polymer as what was assumed.

#### Turbidity of MBBT particle dispersions

MBBT particles have been already extensively studied by light scattering techniques. In [15] the particle size distribution was taken into account when calculating the particle form factor. The MBBT sample used here corresponds to sample B7 in [15], which is representative for the properties of the market product sold as Tinosorb M (BASF). It has been shown in [15]

that the  $d(0.5)$ -result (the median of the particle size distribution) is close to the  $z$ -average of the hydrodynamic diameter. The median value of the MBBT particle dispersion used in this work as measured with the FOQELS method was  $d(0.5) = 130 \pm 11 \text{ nm}$ . With that a hydrodynamic radius of about 65 nm can be expected.

Figure 6 shows a spectrum of MBBT particles at a concentration of 2% (v/w), which corresponds to a volume fraction of  $\varphi = 0.0179$ , measured in a sandwich cuvette of  $d = 0.0008 \text{ cm}$ . The spectrum is an average of 10 measurements with freshly filled cuvettes (standard deviation = 7%). Employing equation (10) the best fit between calculated turbidity and the measured absorbance in the spectral range between 450 and 700 nm was achieved when using a radius ( $R_z$ ) of 66 nm, a value in good agreement with the FOQELS result. In order to perform this calculation the wavelength dependence of the refractive index had to be considered [16]. The data in Table 2 were fitted according to equation (9) by adjusting the parameters to  $a = 0.71827$  and  $b = 0.062443$ . The calculation of the turbidity using equation (10) has to be regarded as an approximation, as the equation applies for the monodisperse case and the sample used here showed a certain polydispersity [15]. Nevertheless, there is good agreement between measured absorbance and calculated turbidity as shown in Figure 6, where the calculated turbidity spectrum is shown for wavelengths equal or longer than 440 nm. The absorption band of the particulate UV absorber MBBT starts to emerge at wavelengths smaller than 440 nm, and the calculation of turbidity then expectedly would deviate from the measured curve. At wavelengths longer than 440 nm the absorbance spectrum of MBBT shown in Figure 6 is only due to scattering.

#### Amplification of absorbance of dyes by polymer spheres

Figure 7 shows spectra of Eosin Yellow at a constant concentration of 0.0174 mM and a cuvette thickness of  $d = 0.1 \text{ cm}$  at different polymer sphere concentrations (%w/v). There is a significant increase of the dye absorbance at increasing particle concentrations. The increase of the absorbance at  $\lambda_{\text{max}} = 517 \text{ nm}$  as function of particle concentration is depicted in Figure 8 for three different dye concentrations, showing also two independent experiments with a dye concentration of 0.0175 mM, which demonstrate good repeatability. The relative increase of dye absorbance is stronger when  $A_0$  is smaller. For further evaluation, turbidities were calculated according to equation (10) with  $\lambda = 517 \text{ nm}$ , a particle radius of  $R = 175 \text{ nm}$ , and the respective volume fraction of the particles. In Figure 9 all results obtained with Eosin Yellow and polymer spheres at various cuvette thicknesses and different initial absorbance of the dye without particles,  $A_0$ , are depicted, showing  $A_p(\lambda)/A_0(\lambda)$  as function of  $(\tau(\lambda) \cdot d/A_0(\lambda))^{1/2}$ . With that kind of plot, all data lie on one single curve. A fit was obtained by adjusting the parameters of the empirical

equation (13) to the experimental data, using the EXCEL solver via a non-linear least squares calculation:

$$y = 1 + \frac{c \cdot x^d}{g + x^d} \quad (13),$$

where  $y = A_p(\lambda)/A_0(\lambda)$ ,  $x = (\tau(\lambda) \cdot d/A_0(\lambda))^{1/2}$  and  $c$ ,  $d$ , and  $g$  are adjustable parameters ( $c = 7.321$ ,  $d = 1.410$ ,  $g = 93.59$ ).

Eosin Yellow has a quite high fluorescence quantum yield of 19% [19]. For that reason similar experiments were performed with other non-fluorescing water-soluble dyes, such as Patent Blue V, Direct Red 254, Evans Blue, and Malachite Green. Figure 10 shows spectra of Patent Blue V at a constant concentration of 0.013 mM and a cuvette thickness of  $d = 0.1$  cm at different polymer sphere concentrations (%w/v). There is a significant increase of dye absorbance with increasing concentration of polymer spheres (Figure 11), as has also been the case for Eosin Yellow. A similar increase is also observed with addition of MBBT particles, also shown in Figure 11. This increase is observed with every dye investigated. For the evaluation of the experiments with the different dyes, absorbance values at the maxima of the absorption spectra of the respective dye were taken, and turbidities were calculated at these wavelengths using a radius for the polymer spheres of  $R = 175$  nm and the respective volume fractions. Evaluated results are depicted in Figure 12. With Malachite Green the maximum absorption was shifted in the presence of the polymer particle from 617 to 630 nm, which might be due to adsorption of the dye to the particles. Again, the fitting curve was calculated using equation (13) and parameters were adjusted, resulting in  $c = 9.096$ ,  $d = 1.989$ , and  $g = 202.9$ . Obviously all results with these four dyes at the different conditions with respect to dye concentration, turbidity due to the presence of polymer spheres, cuvette thickness and different evaluation wavelengths can be drawn on one curve. When comparing Figure 12 with Figure 9, it is evident that this does not apply for the data obtained with Eosin Yellow. At the same value of  $(\tau(\lambda) \cdot d/A_0(\lambda))^{1/2}$  the ratio of  $A_p(\lambda)/A_0(\lambda)$  is smaller with that dye. The reason is most likely the high fluorescence quantum yield of Eosin Yellow, which counteracts the increase of absorbance from scattering of the polymer particles.

#### Amplification of absorbance of a dye by MBBT particles

A similar effect as was observed with systems of dyes and polymer spheres is also observed with dye (Patent Blue V) and MBBT particles. The increase of absorbance of Patent Blue V as function of particle concentration and constant dye concentration was already shown in Figure 11, measured in cuvettes of thickness  $d = 0.1$  cm. The effect of MBBT particles on the absorbance of Patent Blue was also measured in cuvettes of smaller thickness and evaluated in the same manner as with polymer spheres, plotting  $A_p(\lambda)/A_0(\lambda)$  as function of  $(\tau(\lambda) \cdot d/A_0(\lambda))^{1/2}$ , where  $\tau(\lambda)$  was determined

according to equation (10). This relationship is depicted in Figure 13. Equation (13) can again be fitted to these data, using a non-linear least-squares fit, which results in the parameters of  $c = 7.391$ ,  $d = 2.442$ , and  $g = 187.2$ . The form of the curve in Figure 13 is similar to that in Figure 12, but a bit steeper in the linear range of the sigmoidal shape.

#### Conclusions

The data shown in Figures 9, 12 and 13 show that there seems to exist a master-curve for any dye (with the exception of Eosin yellow as already discussed), which is characteristic for a particulate system, when plotting  $A_p(\lambda)/A_0(\lambda)$  against  $(\tau(\lambda) \cdot d/A_0(\lambda))^{1/2}$ . These curves follow a sigmoidal shape, which can be represented by the function of equation (13). Sigmoidal means, that there is no or very little amplification of dye absorbance at low and at high values of  $(\tau(\lambda) \cdot d/A_0(\lambda))^{1/2}$ , whereas in between a region exists, where amplification is approximately linear. The shape of the curve in Figure 13 is similar to that in Figure 12, but steeper in the linear range of the sigmoidal shape. The observed sigmoidal behaviour may be explained with the following considerations. At low values of  $(\tau(\lambda) \cdot d/A_0(\lambda))^{1/2}$  the multiple scattering situation is not yet given, and the postulated random walk diffusion of the scattered light does not apply. So the increase of the pathlength of photons through the sample is negligible. On the other hand, at high values of  $(\tau(\lambda) \cdot d/A_0(\lambda))^{1/2}$  the influence of the structure factor becomes more important, leading to an increased transmittance, which could explain the flattening of the curves. Similar results have been reported by other workers [20], employing Monte Carlo simulations.

The results found in this work could be applied to improve models for the simulation of sun protection factors [21]. Table 3 shows calculations based on the absorbance profile of a sunscreen with sun protection factors (SPF) of 15. The absorbance profile was obtained using a freeware program on the internet [22], and the results of that are listed as  $A_0(\lambda)$  at a range of UV wavelengths. For these wavelengths turbidities were calculated according to equation (10) with 10% (w/v) of polymer spheres. Equation (13) was used with the appropriate parameters given before to determine the amplification factor  $A_p(\lambda)/A_0(\lambda)$ . Table 3 shows, that at higher values of  $A_0(\lambda)$  this factor tends to decrease, so that the impact of the scattering effect will be quite small for sunscreens with higher protection. On the other hand, in the visible and IR-A range, where absorbance is small, this amplification effect may have a stronger influence.

For MBBT particles the effect in the UV range was not calculated as the substance absorbs in the UV, and it is not possible to extrapolate the refractive index into the absorption band with the tools reported here. This and also further consequences for practical sunscreen compositions should be elaborated in future work in more detail.

## Acknowledgements

The authors thank Dr. Oliver Reich and Prof. Dr. Hans-Gerd Löhmannsröben (University of Potsdam, Germany) for helpful discussions and measurements of refractive indices, and as well Nicole Mehnert, Katja Quass, Jochen Giesinger and Hannah Amsler (BASF Grenzach GmbH) for practical help in the laboratory.

## Notes and references

- U. Osterwalder, M. Sohn, B. Herzog. Global state of sunscreens. *Photodermatology, Photoimmunology, Photomedicine*, 2014, **30**, 65 – 81
- B. Herzog. Photoprotection of human skin. *Photochemistry (RSC)*, 2012, **40**, 245 – 273
- U. Osterwalder, B. Herzog. Chemistry and properties of organic and inorganic UV filters. In: *Clinical Guide to Sunscreens and Photoprotection*, ed.: H. W. Lim, Z. D. Draelos, Informa Healthcare, New York 2008, pp. 11 – 38
- D. Schlossmann, Y. Shao. Inorganic ultraviolet filters. In: *Sunscreens - Regulations and Commercial Development*, N. A. Shaath Ed., Cosmetic Science and Technology Series 28, 3rd ed., Taylor & Francis: Boca Raton, 2005, 239 - 279
- B. Herzog, K. Quass, E. Schmidt, S. Müller, H. Luther. Physical properties of organic particulate UV absorbers used in sunscreens. II. UV-attenuating efficiency as function of particle size. *J. Colloid Interface Sci.*, 2004, **276**, 354 - 363
- K. J. Hwang, D.-W. Park, S. Jin, S. O. Kang, D. W. Cho. Influence of dye-concentration on the light-scattering effect in dye-sensitized solar cell. *Materials Chemistry and Physics*, 2015, **149/150**, 594 – 600
- A. Ishimaru. Diffusion of light in turbid material. *Appl. Opt.* 1989, **28**, 2210 – 2215
- A. Einstein. Über die von der molekularkinetischen Theorie der Wärme geforderte Bewegung von in ruhenden Flüssigkeiten suspendierten Teilchen. *Annalen der Physik*, 1905, **17**, 549 – 560
- U. Apfel, R. Grunder, M. Ballauf. A turbidity study of particle interaction in latex dispersions. *Colloid & Polymer Science*, 1994, **272**, 820 – 829
- M. Kerker. The scattering of light and other electromagnetic radiation (Chapter 8). Academic Press, New York, 1969
- M.N. Polyanskiy. *Refractive index database*, <http://refractiveindex.info>. Accessed November 17, 2014
- Lord Rayleigh. On the diffraction of light by spheres of small refractive index. *Proc. Royal Soc. London, Series A: Math, Phys. Eng. Sci.*, 1914, **90**, 219 - 225
- J.K. Percus, G.J. Yevick. Analysis of classical statistical mechanics by means of collective coordinates. *Phys. Rev.* 1958, **110**, 1 – 13
- Ch. E. Jones. Hollow sphere technology for sunscreen formulation. *SOFW Journal*, 2002, **128**, 36 – 40
- B. Herzog, A. Katzenstein, K. Quass, A. Stehlin, H. Luther. Physical properties of organic particulate UV absorbers used in sunscreens. I. Determination of particle size with fiber-optic quasi-elastic light scattering (FOQELS), disc centrifugation, and laser diffractometry. *J. Colloid Interface Sci.*, 2004, **271**, 136 – 144
- O. Reich, H.-G. Löhmannsröben, unpublished data, University of Potsdam (2005)
- H. Wiese, D. Horn. Single-mode fibers in fiber-optic quasielastic light scattering: A study of the dynamics of concentrated latex dispersions. *J. Chem. Phys.* 94 (1991) 6429–6443
- H. Wiese, D. Horn. Fiber-optic quasielastic light scattering in concentrated dispersions: The on-line process control of carotenoid micronization. *Ber. Bunsenges. Phys. Chem.* 1993, **97**, 1589 – 1597
- O. Reich, unpublished data, University of Potsdam (2011)
- L. Bressel, O. Reich. Theoretical and experimental study of the diffuse transmission of light through highly concentrated absorbing and scattering materials. Part I: Monte Carlo simulations. *J. Quantitative Spectroscopy & Radiative Transfer*, 2014, **146**, 190 – 198
- B. Herzog. Models for the calculation of sun protection factors and parameters characterizing the UVA protection ability of cosmetic sunscreens. In: *Colloids in Cosmetics and Personal Care*, ed. Tharwart F. Tadros, Vol. 4, Wiley-VCH, Weinheim, 2008, 275 – 308
- <https://www.screensimulator.basf.com>, used at March 19<sup>th</sup> 2015

## Tables and Figure Captions

Table 1: Refractive index of polymer spheres consisting of a polystyrene (PS) and polymethylmethacrylate (PMMA) copolymer [11]

$\lambda$ (nm)	$n(\text{H}_2\text{O})$	$n(\text{PMMA})$	$n(\text{PS})$	$n(\text{PMMA, PS})^*$	$m(\text{PMMA, PS})$
436	1.3376	1.6170	1.5021	1.5596	1.166
486	1.3356	1.6058	1.4971	1.5515	1.162
546	1.3332	1.5964	1.4928	1.5446	1.159
589	1.3324	1.5915	1.4905	1.5410	1.157
656	1.3310	1.5857	1.4879	1.5368	1.155
707	1.3307	1.5825	1.4864	1.5345	1.153

\* average of  $n(\text{PS})$  and  $n(\text{PMMA})$ ;  $m(\text{PMMA, PS}) = n(\text{PMMA, PS}) / n(\text{H}_2\text{O})$

Table 2: Refractive index of MBBT particles [16]

$\lambda$ (nm)	$n(\text{H}_2\text{O})$	$n(\text{MBBT})$	$m(\text{MBBT})$
436	1.3376	1.930	1.443
486	1.3356	1.870	1.400
546	1.3332	1.840	1.380
589	1.3324	1.820	1.366
656	1.3310	1.810	1.360
707	1.3307	1.800	1.353

Table 3: Example of typical sunscreen absorbance (sun protection factor 15) with 10% of polymer spheres ( $\phi = 0.091$ ) and an average film thickness of 0.002 cm

$\lambda$ (nm)	$A_0(\lambda)$	$\tau$ (1/cm)	$(\tau(\lambda) \cdot d / A_0(\lambda))^{1/2}$	$A_p(\lambda)/A_0(\lambda)$
300	1.189	1851.1	2.01	1.37
320	1.166	1529.7	1.77	1.28
340	0.922	1277.7	1.77	1.28
360	0.803	1079.2	1.70	1.26
380	0.182	921.4	3.24	1.99

## Figure Captions

Fig. 1

Schematic of a sample consisting of an absorbing liquid and scattering particles, with  $I_0$  = intensity of incoming light,  $I_R$  = intensity of back-scattered light,  $I_{TD}$  = intensity of diffuse transmitted light,  $I_t$  = intensity of direct transmitted light)

Fig. 2

a) Detection of direct transmittance for turbidity measurement of particles in the absence of dyes; b) detection of diffuse transmittance for measurements of dye absorbance in the presence of particles

Fig. 3

Visible light spectra of dyes used; measurements without integrating sphere at  $d = 1$  cm,  $c(\text{Direct Red 254}) = 0.0136$  mM,  $c(\text{Eosin Yellow}) = 0.0042$  mM,  $c(\text{Evans Blue}) = 0.0040$  mM,  $c(\text{Malachite Green}) = 0.0016$  mM,  $c(\text{Patent Blue V}) = 0.0026$  mM

Fig. 4

Particle form factor of spherical polymer; open circles refer to measurements, solid line to calculations using equation (11) and  $R = 175$  nm

Fig. 5

Absorbance spectrum of spherical polymer with  $d = 0.1$  cm; symbols correspond to measurements of  $A(\lambda)$  without integrating sphere, solid line to calculations of  $\tau(\lambda) \cdot d / \ln 10$  with  $R = 175$  nm at  $\varphi = 0.001769$  and  $d = 0.1$  cm according to equation (10)

Fig. 6

Absorbance spectrum of MBBT particles; dashed line represents measurements of  $A(\lambda)$  without integrating sphere, solid line calculations of  $\tau(\lambda) \cdot d / \ln 10$  with  $R = 66$  nm at  $\varphi = 0.0179$  and  $d = 0.0008$  cm according to equation (10)

Fig. 7

Spectra of Eosin Yellow at constant concentration of 0.0174 mM and a cuvette thickness of  $d = 0.1$  cm at different polymer sphere concentrations (%w/v)

Fig. 8

Increase of absorbance of Eosin Yellow at constant concentrations of 0.0093 mM, 0.0174 mM, and 0.0325 mM, respectively, and a cuvette thickness of  $d = 0.1$  cm, as function of polymer sphere concentration (% w/v); two independent measurements with 0.0174 mM Eosin Yellow

Fig. 9

Amplification of absorbance with Eosin Yellow at a variety of initial absorbance values and cuvette thicknesses measured at  $\lambda = 517$  nm

Fig. 10

Spectra of Patent Blue V at a constant concentration of 0.013 mM and an optical pathlength of  $d = 0.1$  cm at different polymer sphere concentrations (%w/v)

Fig. 11

Increase of absorbance of Patent Blue V at constant concentration of 0.013 mM or 0.0148 mM, respectively, and a cuvette thickness of  $d = 0.1$  cm as function of polymer spheres or MBBT particle concentration (% w/v) at  $\lambda = 637$  nm

Fig. 12

Amplification of absorbance of different dyes with polymer spheres; data from a variety cuvette thicknesses and initial absorbance values (Evans Blue at 604 nm, Malachite Green at 630 nm, Direct Red at 504 nm, Patent Blue at 637 nm)

Fig. 13

Amplification of absorbance of Patent Blue V by MBBT particles; data obtained with different cuvette thicknesses

Fig. 1:

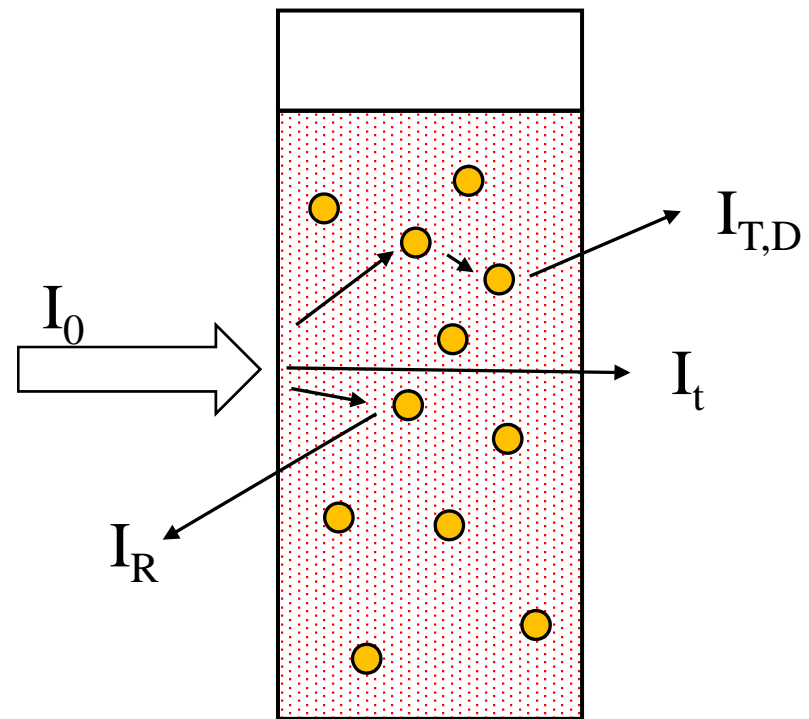


Fig. 2:

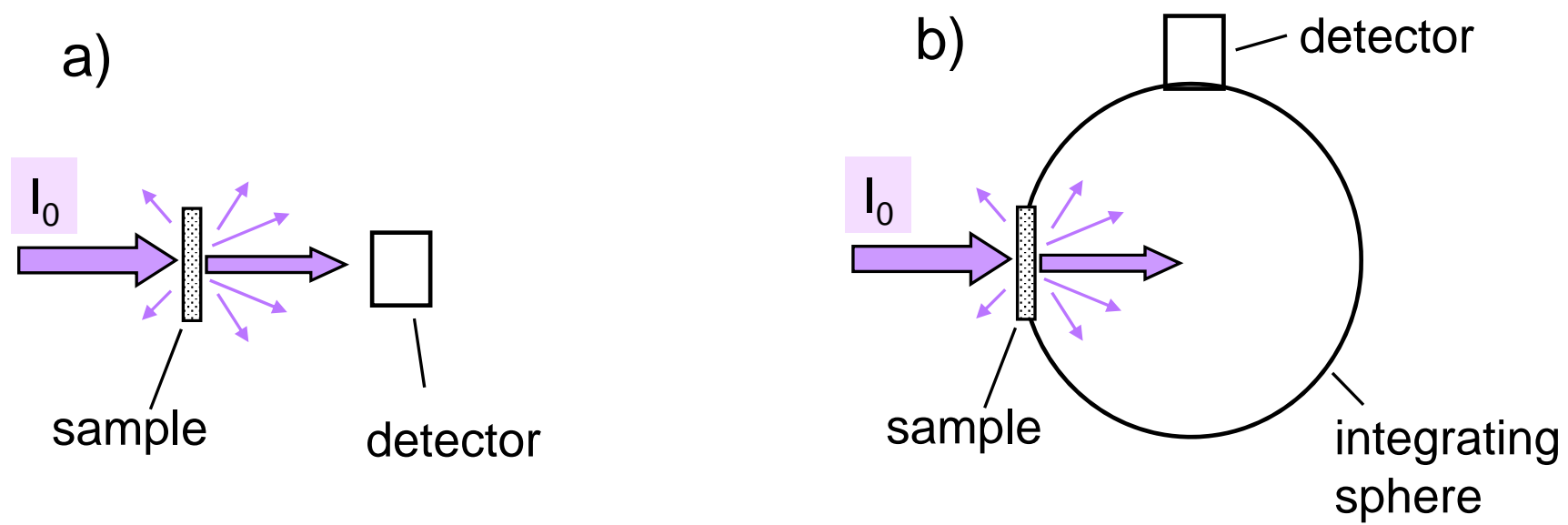


Fig. 3:

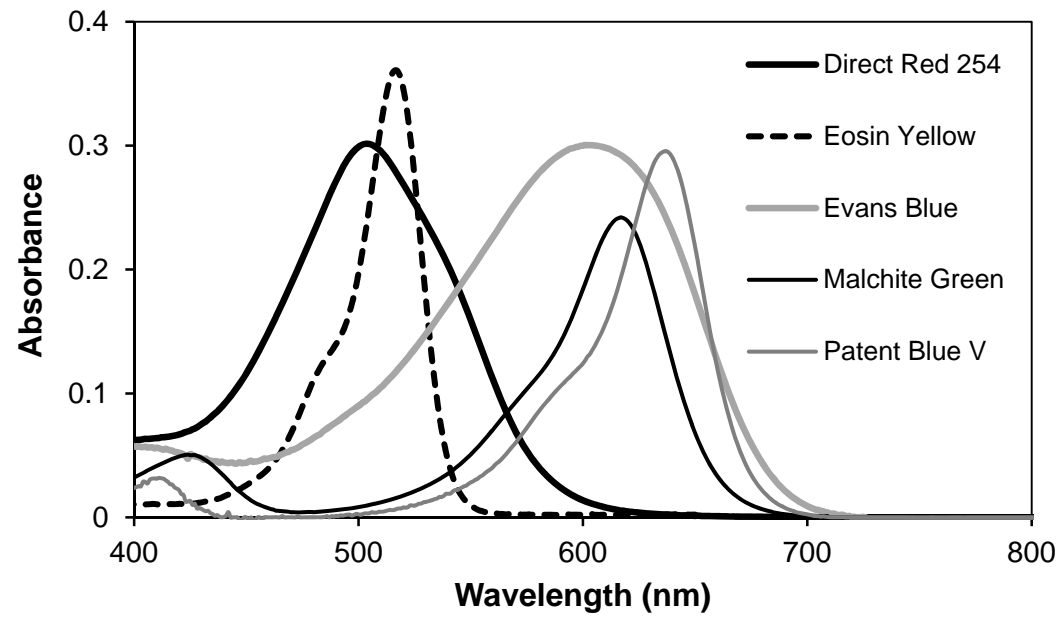


Fig. 4:

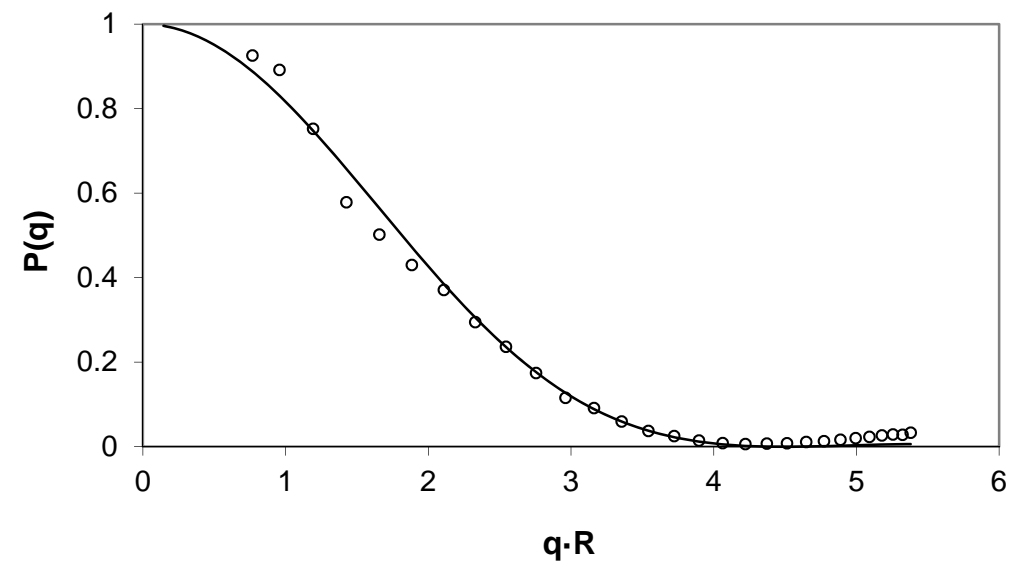


Fig. 5:

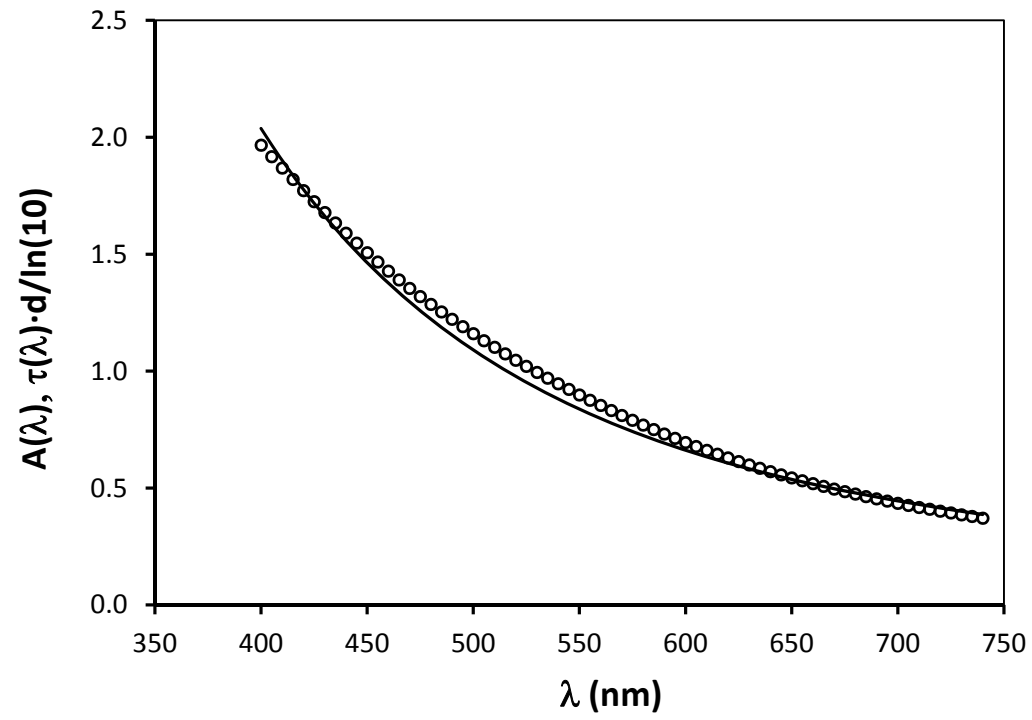


Fig. 6:

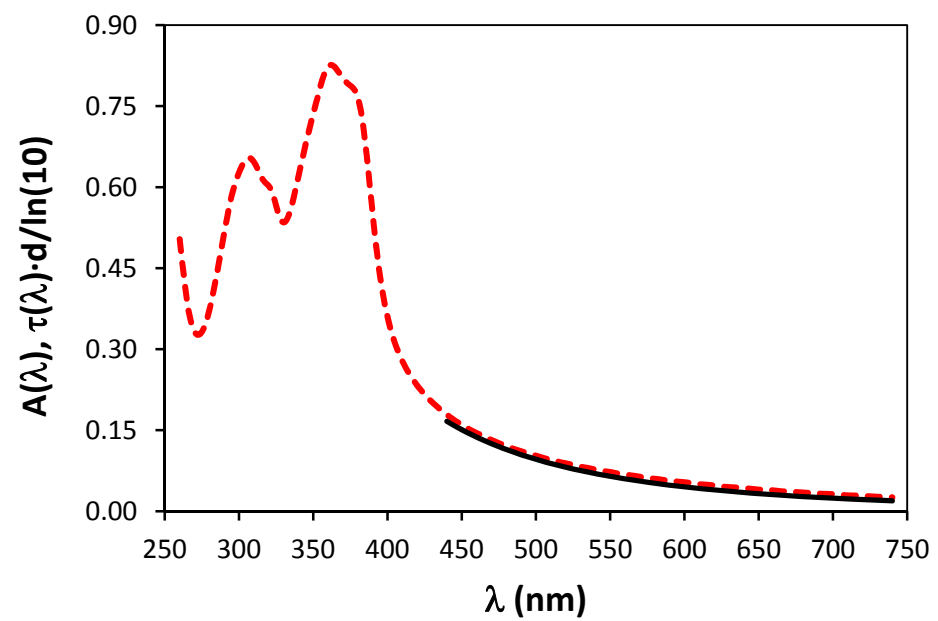


Fig. 7:

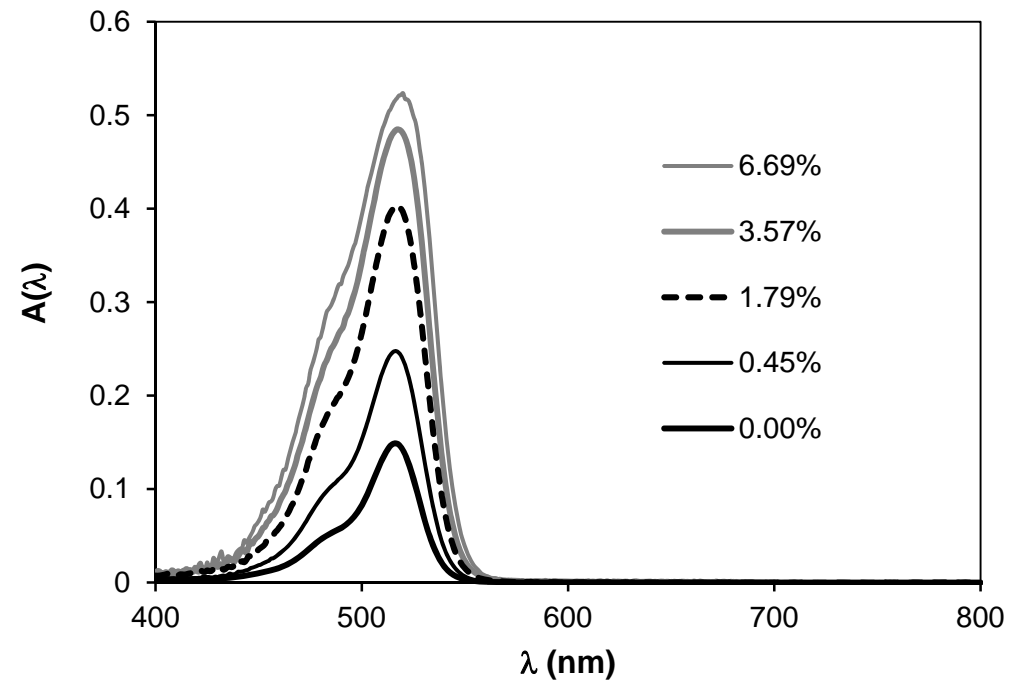


Fig. 8:

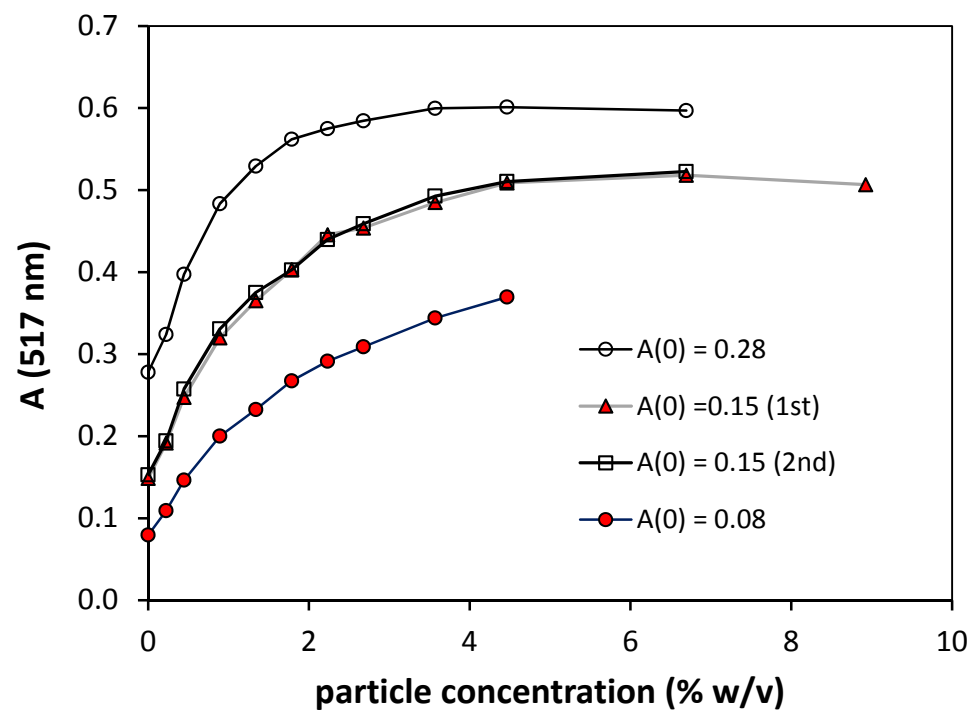


Fig. 9:

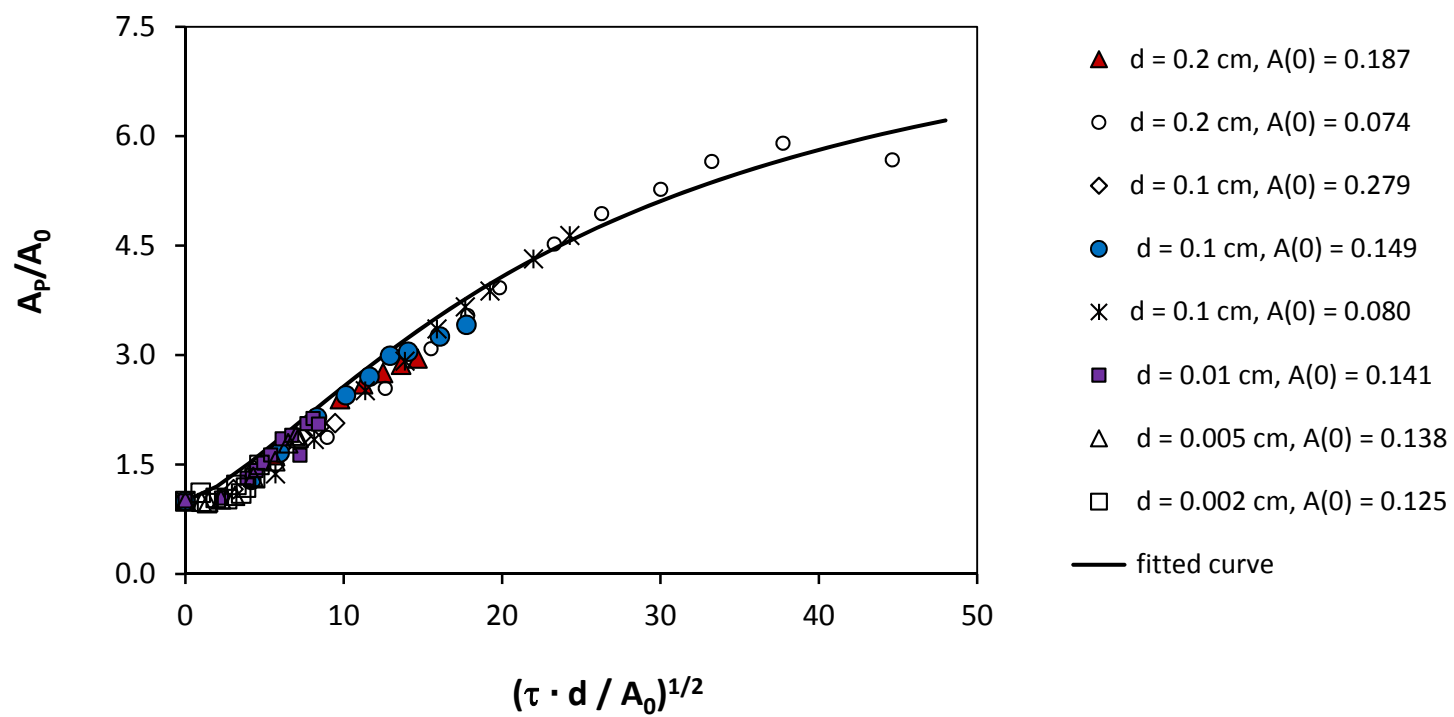


Fig. 10:

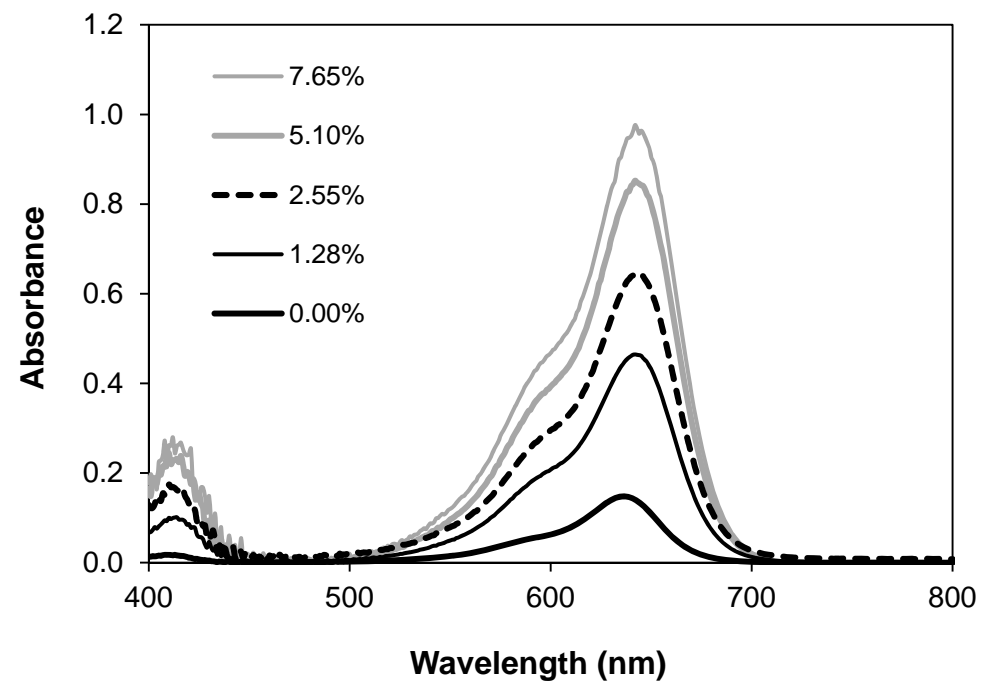


Fig. 11:

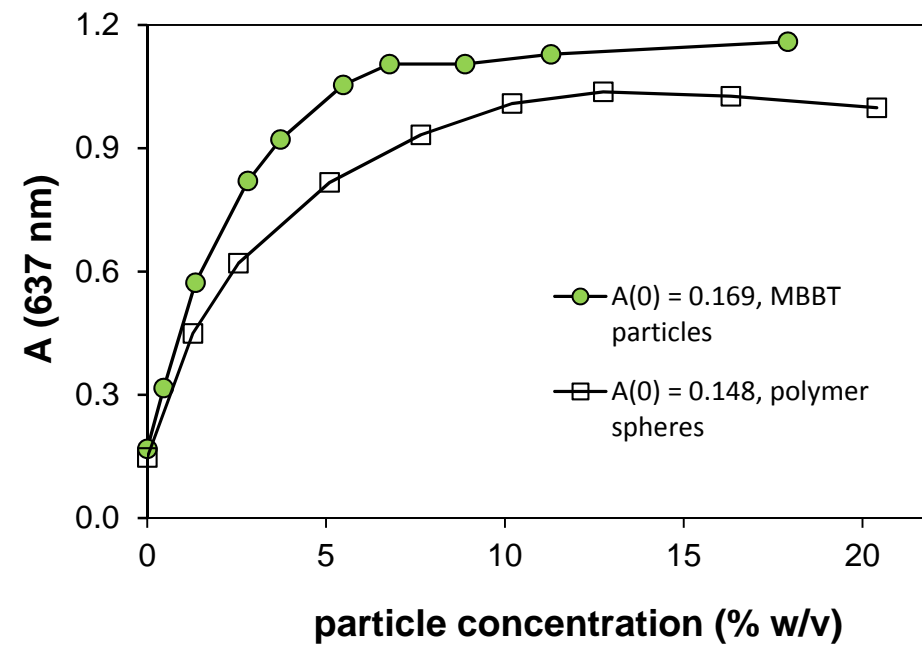


Fig. 12:

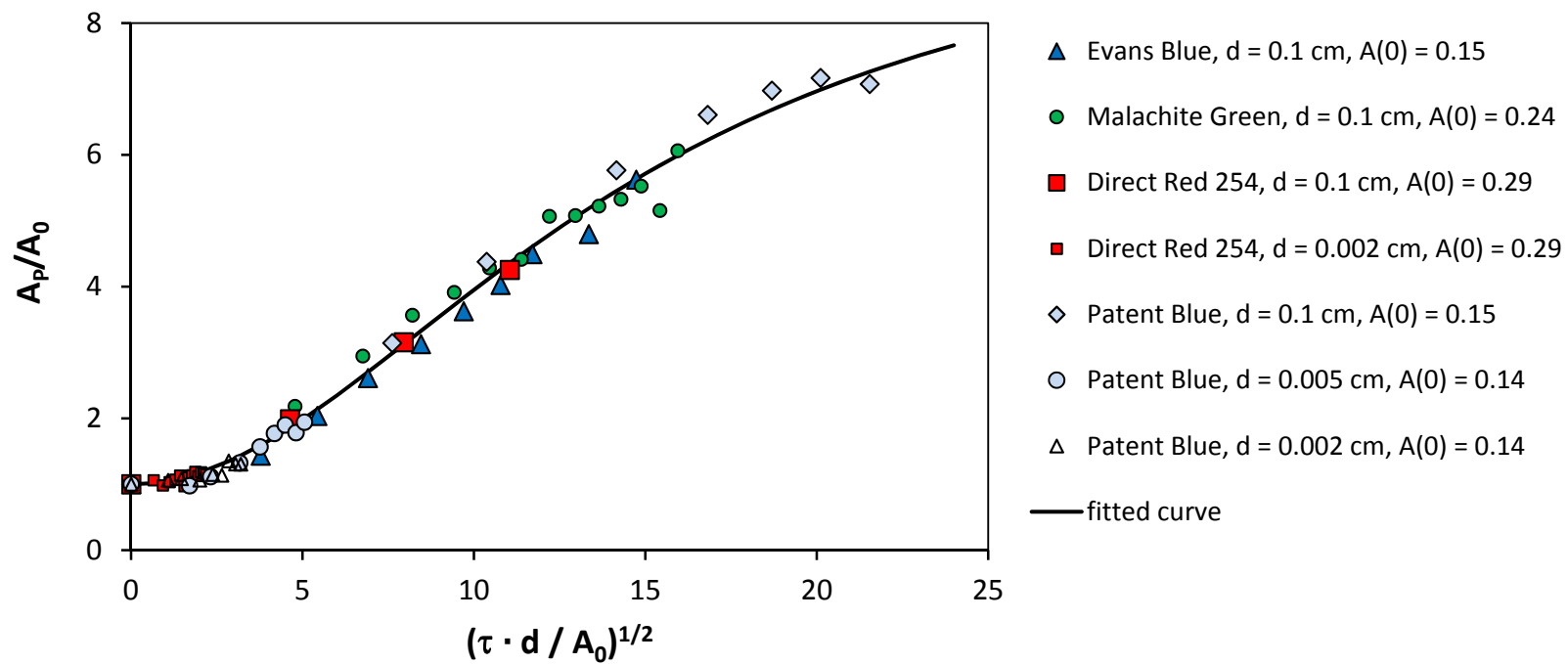
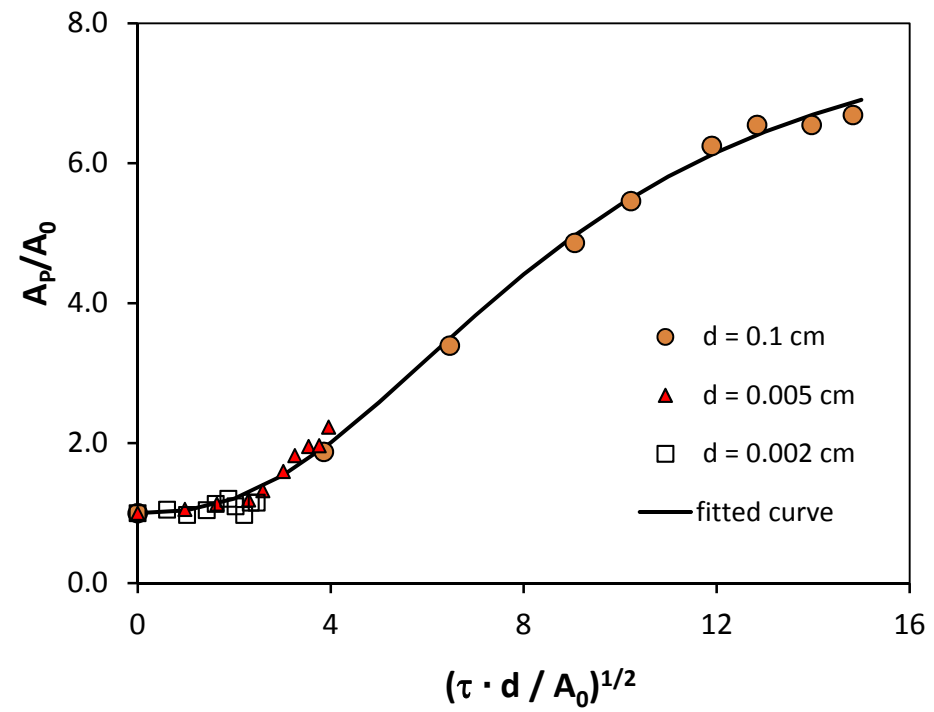


Fig. 13:



## Graphical abstract

Scattering particles increase the absorbance of dyes dissolved in the same medium. This principle can also be applied to sunscreens, which often contain inorganic or organic particles as well as soluble UV absorbers.

